Phase control of iridium and iridium oxide thin films in atomic layer deposition

Sung-Wook Kim, Se-Hun Kwon, Dong-Kee Kwak, and Sang-Won Kang[a)]
Department of Materials Science and Engineering, Korea Advanced Institute of Science and Technology, #373-1 Guseong-dong, Yuseong-gu, Daejeon 305-701, Republic of Korea

(Received 19 July 2007; accepted 23 November 2007; published online 28 January 2008)

The atomic layer deposition of iridium (Ir) and iridium oxide (IrO_2) films was investigated using an alternating supply of (ethylcyclopentadienyl)(1,5-cyclooctadiene) iridium and oxygen gas at temperatures between 230 and 290 °C. The phase transition between Ir and IrO_2 occurred at the critical oxygen partial pressure during the oxygen injection pulse. The oxygen partial pressure was controlled by the $O_2/(Ar+O_2)$ ratio or deposition pressures. The resistivity of the deposited Ir and IrO_2 films was about 9 and 120 $\mu\Omega$ cm, respectively. In addition, the critical oxygen partial pressure for the phase transition between Ir and IrO_2 was increased with increasing the deposition temperature. Thus, the phase of the deposited film, either Ir or IrO_2, was controlled by the oxygen partial pressure and the deposition temperature. However, the formation of a thin Ir layer was detected between the IrO_2 and SiO_2 substrate. To remove this interfacial layer, the oxygen partial pressure is increased to a severe condition. And the impurity contents were below the detection limit of Auger electron spectroscopy in both Ir and IrO_2 films. © *2008 American Institute of Physics*. [DOI: 10.1063/1.2836965]

I. INTRODUCTION

Perovskite materials, such as $SrTiO_3$, $(Ba,Sr)TiO_3$, $Pb(Zr,Ti)O_3$, and $SrBi_2Ta_2O_9$, are widely studied for the application in dynamic random access memory (DRAM) and ferroelectric random access memory (FRAM) devices.[1–4] These materials require a high temperature process in oxygen ambient for the deposition or crystallization of the films. Moreover, underlying layers such as a poly-Si plug or a TiN barrier could be exposed to oxygen to be oxidized due to the penetration of oxygen into the electrode materials during this highly oxidizing ambient. And thus, the bottom electrode materials, which remain conductive in the highly oxidizing ambient and also prevent diffusion of oxygen to protect underlying layers, are required.[5]

Ruthenium (Ru) is a widely studied electrode material due to its formation of conductive ruthenium oxide (RuO_2), low resistivity, and ability to block the diffusion of oxygen into the underlying layer during heat treatment.[6] However, Ru and RuO_2 readily form the volatile species, such as RuO_3 and RuO_4, during high temperature annealing. Above the temperature of 700 °C, the film degradation of a RuO_2/Ru stacked structure was reported due to the formation of the volatile species.[7] Therefore, electrode materials that are more stable at a high temperature in oxygen ambient are required. Iridium (Ir) and its conductive oxide, iridium oxide (IrO_2), are also one of the potential electrode materials. Ir and IrO_2 also have low resistivity and good oxygen barrier properties, like Ru and RuO_2.[6] Compared to Ru, the volatile phases of Ir form at a temperature above 1200 °C,[8] which means that Ir and IrO_2 remain more stable than Ru and RuO_2 during the high temperature process in oxygen ambient.

To integrate giga-bit-scale DRAMs and FRAMs, the capacitors need a three-dimensional structure to increase the total capacitor area. In such structures, it is difficult to deposit electrode and perovskite materials conformally in all capacitor areas using conventional deposition techniques, such as physical vapor deposition and chemical vapor deposition (CVD). Therefore, the atomic layer deposition (ALD) technique providing excellent conformality is required to fabricate Ir or IrO_2 films as a capacitor electrode material.[9,10] However, the ALD processes for Ir and IrO_2 were not studied extensively, yet. Although some ALD processes for single-phase Ir and IrO_2 have been described,[11–14] no ALD process focusing on the controlling of Ir and IrO_2 has been reported.

In this paper, an ALD process for IrO_2 as well as Ir was presented using (ethylcyclopentadienyl)(1,5-cyclooctadiene) iridium [Ir(EtCp)(COD)] as an Ir precursor and oxygen as a reactant gas. To control the phase of the deposited films, the $O_2/(Ar+O_2)$ ratio during the oxygen injection pulse, deposition pressure, and deposition temperature were controlled.

II. EXPERIMENT

Ir and IrO_2 films were deposited on a 100-nm-thick SiO_2/Si substrate at deposition temperatures from 230 to 290 °C using an alternating supply of Ir(EtCp)(COD) and oxygen gas. Ir(EtCp)(COD) was contained in a bubbler, which is heated to 85 °C, and was delivered to reactor by argon carrier gas at a flow rate of 50 sccm. The feeding line was heated to 100 °C to prevent condensation of the Ir precursor. Deposition pressures were varied from 1 to 5 Torr. One deposition cycle of Ir and IrO_2 ALD consisted of four sequences: (i) an exposure of Ir(EtCp)(COD), (ii) a purge pulse with 50 sccm argon, (iii) an exposure of oxygen gas mixed with argon, and (iv) another purge with 50 sccm argon. This cycle is repeated as many times as necessary to obtain the desired film thickness. During the oxygen pulse,

[a)]Electronic mail: swkang@kaist.ac.kr.

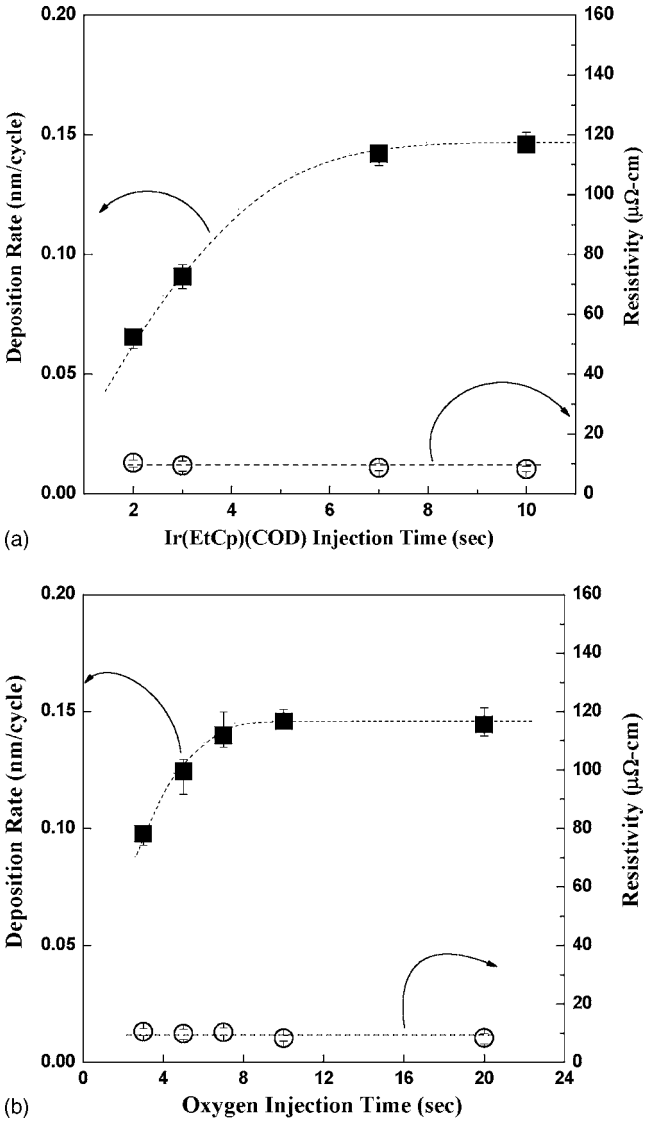

FIG. 1. The dependence of the deposition rate and the resistivity of the film on the (a) Ir(EtCp)(COD) injection time at the fixed oxygen injection time of 10 s and (b) the oxygen injection time at the fixed Ir(EtCp)(COD) injection time of 10 s. The $O_2/(Ar+O_2)$ ratio was fixed to 54.5% at a deposition temperature of 290 °C under a deposition pressure of 1 Torr.

the oxygen flow rate was fixed to 120 sccm and the argon flow rate was varied from 0 to 150 sccm to control the $O_2/(Ar+O_2)$ ratio from 44.4% to 100%. The thickness of the deposited films was determined using field-emission scanning electron microscopy. The resistivity of the films was calculated from the sheet resistance measured by the four point probe and the film thickness. X-ray diffraction (XRD) analysis was used to determine the crystal structure of the deposited films. The composition of the films was measured using Auger electron spectroscopy (AES).

III. RESULTS AND DISCUSSION

Figure 1(a) shows the dependence of the deposition rate and resistivity of the films on the Ir(EtCp)(COD) injection time at a deposition temperature of 290 °C under a deposition pressure of 1 Torr. The Ir(EtCp)(COD) injection time was varied from 2 to 10 s. The oxygen injection time was

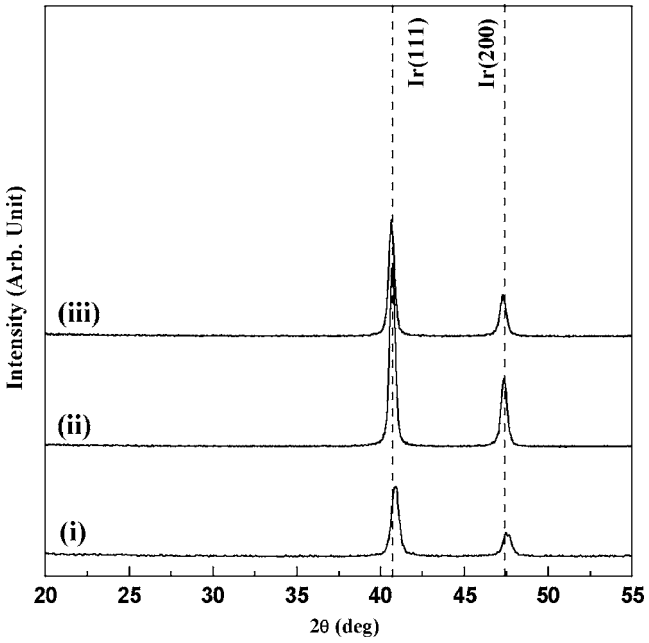

FIG. 2. The XRD patterns obtained from deposited films in cases of (i) Ir(EtCp)(COD) injection for 7 s and oxygen injection for 10 s, (ii) Ir(EtCp)(COD) injection for 10 s and oxygen injection for 10 s, and (iii) Ir(EtCp)(COD) injection for 10 s and oxygen injection for 20 s, respectively. The $O_2/(Ar+O_2)$ ratio was fixed to 54.5% at a deposition temperature of 290 °C under a deposition pressure of 1 Torr.

fixed to 10 s and the $O_2/(Ar+O_2)$ ratio during the oxygen injection pulse was fixed to 54.5%. Figure 1(b) shows the dependence of the deposition rate and resistivity of the deposited films on the oxygen injection time at the same deposition conditions. The oxygen injection time was varied from 2 to 20 s and the Ir(EtCp)(COD) injection time was fixed to 10 s. The deposition rate of the film was saturated at about 0.145 nm/cycle after both an Ir(EtCp)(COD) and oxygen injection time of 7 s. This means that the film deposition follows ALD characteristic, self-limiting behavior, also. The resistivity of the deposited film was about 9 $\mu\Omega$ cm. XRD analysis confirmed that the phase of the deposited film was only metallic Ir regardless of the Ir(EtCp)(COD) and the oxygen injection times as shown in Fig. 2. The phase of deposited films was independent on the precursor and oxygen injection time in this condition, an $O_2/(Ar+O_2)$ ratio of 54.5%. This indicates that oxygen molecules break the chemical bonding between Ir atoms and organic ligands of Ir(EtCp)(COD) but do not react with Ir atoms at a given $O_2/(Ar+O_2)$ ratio.

To deposit IrO_2 films, the $O_2/(Ar+O_2)$ ratio was varied from 44.4% to 100% at a deposition temperature of 290 °C under a deposition pressure of 1 Torr. Both Ir(EtCp)(COD) and oxygen injection times were fixed to 10 s. Figure 3(a) shows the dependence of the deposition rate and the resistivity of the film on the $O_2/(Ar+O_2)$ ratio. The deposition rate and resistivity increased drastically at the $O_2/(Ar+O_2)$ ratio of 75%. The deposition rate was about 0.47 nm/cycle and the resistivity was about 120 $\mu\Omega$ cm. XRD analysis indicated that IrO_2 was formed above an $O_2/(Ar+O_2)$ ratio of 75%, as shown in Fig. 3(b). This means that the abrupt change of the deposition rate and the resistivity is due to the formation of

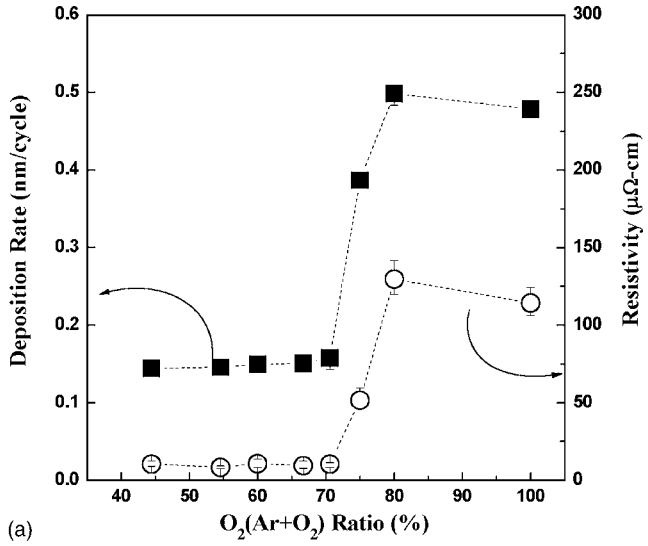

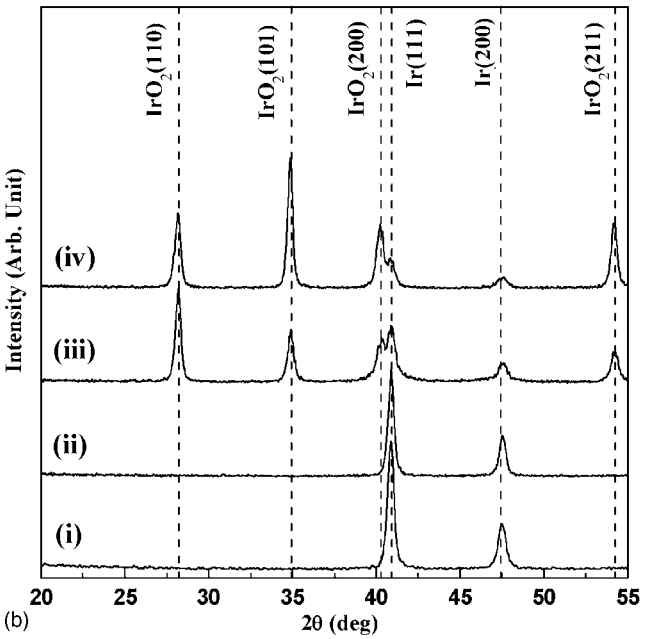

FIG. 3. (a) The dependence of the deposition rate and the resistivity of the film on the $O_2/(Ar+O_2)$ ratio. (b) The XRD patterns obtained from deposited films in cases of an $O_2/(Ar+O_2)$ ratio of (i) 44.4%, (ii) 66.6%, (iii) 80%, and (iv) 100%. A deposition temperature was 290 °C under a deposition pressure of 1 Torr. Both the Ir(EtCp)(COD) and oxygen injection time were fixed to 10 s.

IrO_2 at a high $O_2/(Ar+O_2)$ ratio. The deposition rate and the resistivity were also independent on Ir(EtCp)(COD) injection time from 10 to 20 s at the $O_2/(Ar+O_2)$ ratio of 100%, where IrO_2 was formed, as shown in Fig. 4. This means that an Ir(EtCp)(COD) injection time of 10 s is enough time for the saturation of both Ir and IrO_2 films, and thus the precursor injection time was fixed to 10 s. The deposition rate of IrO_2 films, 0.47 nm/cycle, was about three times higher than that of Ir films, 0.145 nm/cycle. The crystal structure of Ir is a face-centered-cubic structure which has a lattice constant of 3.83 Å and four Ir atoms are contained in the unit cell. However, the crystal structure of IrO_2 is a tetragonal rutile structure which has a lattice constant of $a=4.50$ Å and $c=3.15$ Å and two Ir atoms and four oxygen atoms are contained in the unit cell. Hence, the volume of IrO_2 is about 2.27 times higher than that of Ir when the films have the same number of Ir atoms. But this value is still smaller than the increment ratio of the deposition rate. Another reason for the increment of the deposition rate might be the increment of an amount of adsorbed Ir precursor. In the case of Ru and RuO_2 using bis(ethylcyclopentadienyl) ruthenium $[Ru(EtCp)_2]$, the amount of the adsorbed precursor of RuO_2 is larger than that of Ru.[15] Like this, IrO_2 may have more adsorption site of Ir(EtCp)(COD) than Ir, which leads to an increase of the deposition rate.

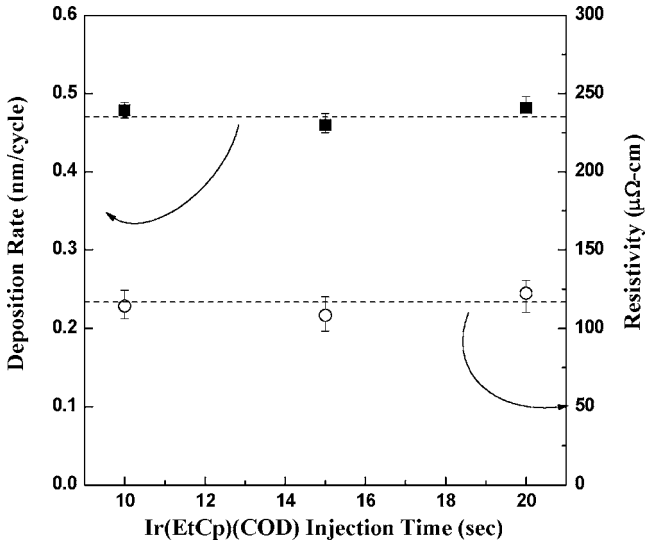

FIG. 4. The dependence of the deposition rate and the resistivity of the film on the Ir(EtCp)(COD) injection time at the fixed $O_2/(Ar+O_2)$ ratio of 100% and oxygen injection time of 10 s at a deposition temperature of 290 °C under a deposition pressure of 1 Torr.

As mentioned earlier, IrO_2 films were obtained at a high $O_2/(Ar+O_2)$ ratio. At a high $O_2/(Ar+O_2)$ ratio, both the oxygen partial pressure and oxygen dosage impinging on the surface are increased and these two factors can enhance the formation of IrO_2 films. To clarify what the dominant factor that determines the phase of the deposited film is, the oxygen injection time was increased to increase the oxygen dosage impinging on the surface at the Ir formation condition. Figure 5 shows that the deposition rate and resistivity were independent on the oxygen injection time at an $O_2/(Ar+O_2)$ ratio of 54.5% until 90 s. While the oxygen dosage impinging on the surface in case of an $O_2/(Ar+O_2)$ ratio of 54.5% and an oxygen injection time of 90 s is about 4.9×10^7 L, the oxygen dosage impinging on the surface in case of an $O_2/(Ar+O_2)$ ratio of 75% and an oxygen injection time of 10 s is about 7.5×10^6 L and this is a lower value than the former case. This indicates that the transition between Ir and IrO_2 is mainly determined not by the oxygen dosage impinging on the surface but by the oxygen partial pressure.

To confirm the effect of the oxygen partial pressure on the transition between Ir and IrO_2, a two-step ALD was designed. The two-step ALD, separation of the Ir formation step and oxidation step, consists of six sequences: (i) an exposure of Ir(EtCp)(COD), (ii) a purge pulse, (iii) an exposure of oxygen gas at a low $O_2/(Ar+O_2)$ ratio to deposit Ir, (iv) a purge pulse, (v) an exposure of oxygen gas at a high

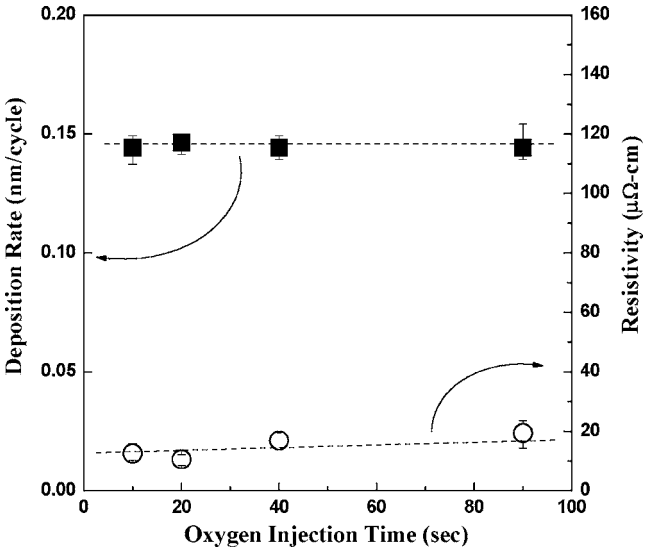

FIG. 5. The dependence of the deposition rate and the resistivity on the oxygen injection time from 10 to 90 s. The Ir(EtCp)(COD) injection time was fixed to 10 s and the $O_2/(Ar+O_2)$ ratio was 54.5% at a deposition temperature of 290 °C under a deposition pressure of 1 Torr.

$O_2/(Ar+O_2)$ ratio to oxidize deposited Ir, and (vi) a purge pulse. In step 1, Ir formation step, after the Ir(EtCp)(COD) injection and argon purge, oxygen with an $O_2/(Ar+O_2)$ ratio of 54.5% was injected for 10 s to deposit the Ir film. And in step 2, Ir oxidation step, oxygen with an $O_2/(Ar+O_2)$ ratio of 100% was injected for 10 s to oxidize the deposited Ir. As a result of the two-step ALD, the deposition rate and resistivity were identical compared to the case of the conventional ALD of Ir at an $O_2/(Ar+O_2)$ ratio of 54.5%, which indicates that the oxidation reaction of the deposited Ir did not occurred at a high $O_2/(Ar+O_2)$ ratio. This means that the reaction path for the deposition of IrO_2 is not a two-step reaction from Ir(EtCp)(COD) to Ir, and from Ir to IrO_2, but a direct reaction from Ir(EtCp)(COD) to IrO_2.

As for another method for the deposition of IrO_2, the deposition pressures were varied from 1 to 5 Torr at a deposition temperature of 290 °C for an $O_2/(Ar+O_2)$ ratio of 54.5%. While the $O_2/(Ar+O_2)$ ratio is same, the higher deposition pressure makes the absolute value of the oxygen partial pressure higher than the low deposition pressure because the oxygen partial pressure is expressed by multiplication of a mole fraction of oxygen in a reaction chamber and total pressure. As shown in Fig. 6(a), the deposition rate and resistivity of the deposited films increased at high deposition pressure, indicating the formation of IrO_2 films. Compared to a high $O_2/(Ar+O_2)$ ratio at a deposition pressure of 1 Torr as shown in Fig. 3, the deposition rate and resistivity were almost identical. Figure 6(b) also shows that formation of IrO_2 films at high deposition pressure. From the earlier results, increasing an $O_2/(Ar+O_2)$ ratio or the deposition pressure to obtain IrO_2 films, it is demonstrated that the oxygen partial pressure is a dominant factor for the transition between Ir and IrO_2.

Figure 7(a) shows the dependence of the resistivity of the deposited films on the $O_2/(Ar+O_2)$ ratio at deposition temperatures of 230–290 °C. At all temperature ranges, an

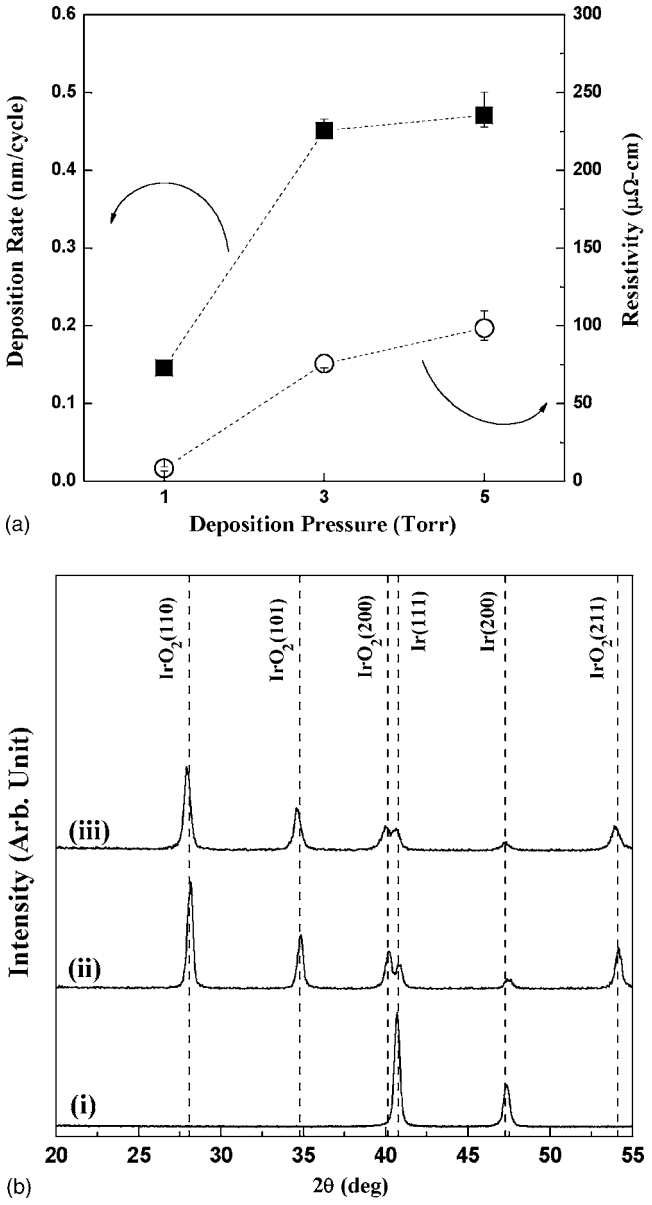

FIG. 6. (a) The dependence of the deposition rate and the resistivity of the deposited film on deposition pressures from 1 to 5 Torr. (b) The XRD patterns obtained from deposited films on deposition pressures of (i) 1, (ii) 3, and (iii) 5 Torr. A deposition temperature was 290 °C and the $O_2/(Ar+O_2)$ ratio was fixed to 54.5%.

increment of the resistivity of the deposited films depending on the $O_2/(Ar+O_2)$ ratio was observed and this means that the deposition of Ir and IrO_2 can be controlled at wide temperature ranges. The ALD of IrO_2 was achieved at a low deposition temperature of 230 °C, which is lower than the value for the CVD of IrO_2.[16–18] As deposition temperatures increased, the $O_2/(Ar+O_2)$ ratio for the transition between Ir and IrO_2 also increased, demonstrating that the deposition of Ir and IrO_2 can be also controlled by deposition temperatures at the same deposition pressure and $O_2/(Ar+O_2)$ ratio. At low deposition temperature, it is easier to form IrO_2 even at a low oxygen partial pressure, as shown in Fig. 7(a). The phase equilibrium of Ir and IrO_2 is determined by temperature and oxygen pressure.[19,20] The critical oxygen pressure for the equilibrium of Ir and IrO_2 is controlled by the tem-

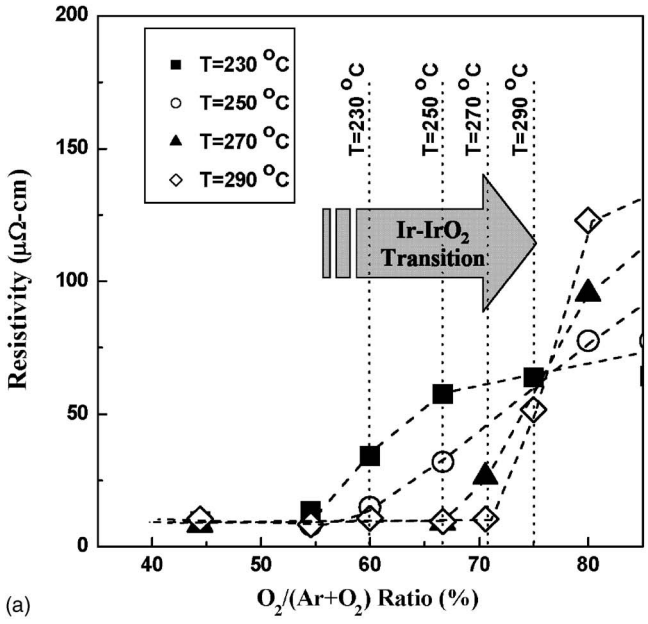

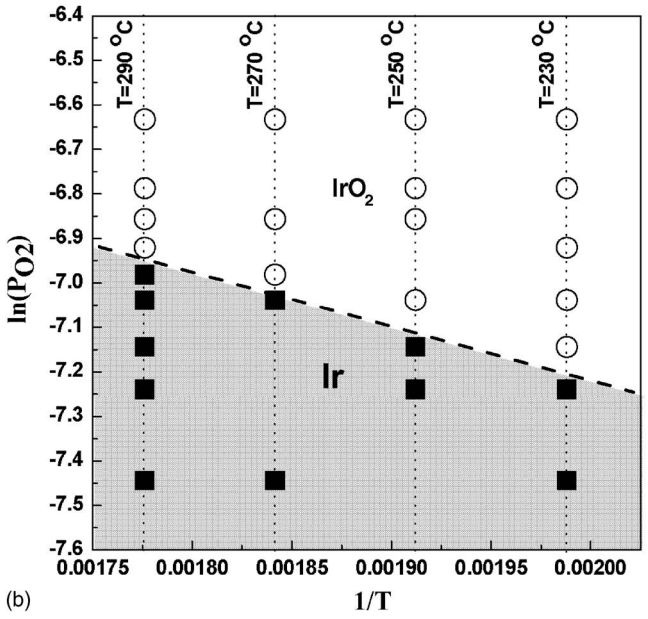

FIG. 7. (a) The dependence of the resistivity of the film on the $O_2/(Ar+O_2)$ ratio at deposition temperatures from 230 to 290 °C under a deposition pressure of 1 Torr. (b) The dependence of the oxygen partial pressure for transition between Ir and IrO_2 on the deposition temperature.

perature from the thermodynamic relationship. Generally, the relationship between the critical oxygen pressure $(P^*_{O_2})$ and temperature (T) is expressed by

$$\ln P^*_{O_2} = -\frac{1}{R}\left(\frac{A}{T} + B + C \log T\right), \quad (1)$$

where R is the gas constant, and A, B, and C are constants.[20] Figure 7(b) shows the dependence of the oxygen partial pressure for the equilibrium of Ir and IrO_2 on deposition temperatures. The $\ln P_{O_2}$ is proportional to $1/T$, also.

In every case shown earlier, XRD patterns of all IrO_2 films still have the metallic Ir peaks as shown in Figs. 6(b). From the AES depth profile shown in Fig. 8, a thin Ir interfacial layer between SiO_2 and IrO_2 was confirmed. At the

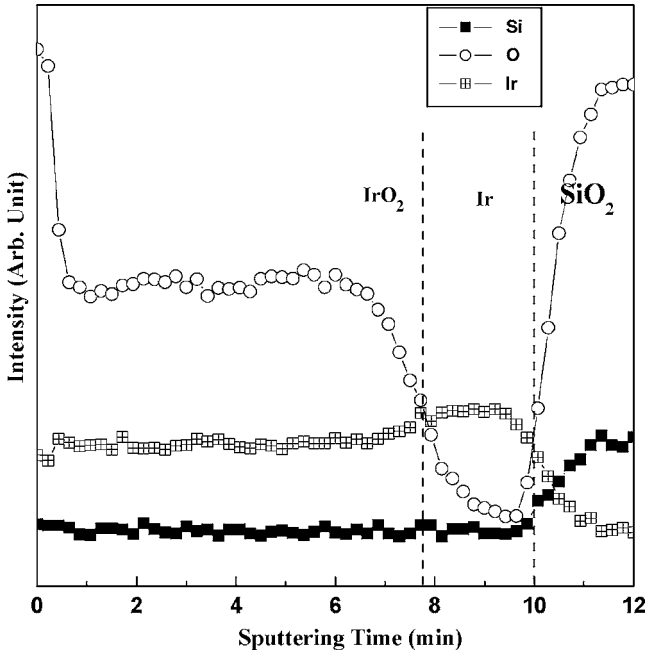

FIG. 8. AES depth profile of IrO_2 film. The $O_2/(Ar+O_2)$ ratio was fixed to 66.6% at a deposition temperature of 230 °C under a deposition pressure of 3 Torr.

initial stage of deposition, metallic Ir was deposited prior to the deposition of IrO_2 on the SiO_2 surface. As the deposition progressed, IrO_2 films started to be deposited after the SiO_2 surface was fully covered with Ir. To remove this interfacial layer, a deposition temperature was decreased to 230 °C because critical oxygen partial pressure is the lowest at this temperature. And to increase the oxygen partial pressure, a deposition pressure was also increased to 3 Torr. Figure 9 shows the XRD patterns of the deposited films depending on the $O_2/(Ar+O_2)$ ratio. At an $O_2/(Ar+O_2)$ ratio of 100%, an

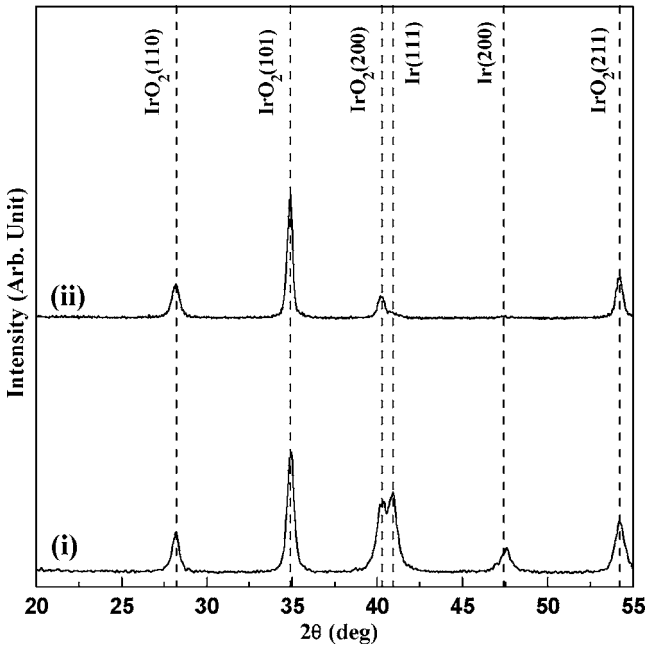

FIG. 9. XRD patterns obtained from deposited film in case of (i) the $O_2/(Ar+O_2)$ ratio of 66.6% and (ii) the $O_2/(Ar+O_2)$ ratio of 100% at a deposition temperature of 230 °C under a deposition pressure of 3 Torr.

almost Ir-free IrO_2 film was obtained. This means that at the initial stage of deposition on the SiO_2 surface, more oxygen partial pressure is needed to deposit IrO_2 films directly without the deposition of an Ir interfacial layer. In other words, the transition conditions from Ir to IrO_2 obtained from previous results are the conditions on the Ir surface, not on the SiO_2 surface. This difference of the transition condition depending on substrate materials might be due to a lattice mismatch, surface adsorption characteristics, or any other factors. To clarify this phenomenon, more study will be needed.

The film composition was determined using AES. The carbon and oxygen impurities in the Ir films were below the AES detection limit and the carbon impurities in the IrO_2 films were also below the AES detection limit.

IV. CONCLUSIONS

The Ir and IrO_2 films were deposited by ALD using Ir(EtCp)(COD) and oxygen gas at deposition temperatures from 230 to 290 °C. The deposition of Ir and IrO_2 can be controlled by controlling the $O_2/(Ar+O_2)$ ratio, deposition pressures, and deposition temperatures. The deposition rate and the resistivity of Ir film were about 0.145 nm/cycle and 9 $\mu\Omega$ cm at a low $O_2/(Ar+O_2)$ ratio at a deposition temperature of 290 °C under a deposition pressure of 1 Torr. And the deposition rate and the resistivity of IrO_2 film were about 0.47 nm/cycle and 120 $\mu\Omega$ cm at a high $O_2/(Ar+O_2)$ ratio at the same deposition temperature and pressure due to the formation of IrO_2. The deposition rate and the resistivity also increased when deposition pressures were increased at the same $O_2/(Ar+O_2)$ ratio and the same deposition temperature. In both cases, the increment of the oxygen partial pressure leads to the transition between Ir and IrO_2 due to the change of the reaction path between Ir(EtCp)(COD) and oxygen not the oxidation of deposited Ir at the high oxygen partial pressure. As deposition temperatures were increased, the critical oxygen partial pressure for the transition between Ir and IrO_2 was also increased. And thus the control of Ir and IrO_2 can also be achieved by the control of the deposition temperatures at the same deposition pressure and $O_2/(Ar+O_2)$ ratio. However, the Ir interfacial layer was formed between the IrO_2 and SiO_2 substrate in almost all the cases. To remove this interfacial layer, the oxygen partial pressure is increased to a severe condition, which is an $O_2/(Ar+O_2)$ ratio of 100% at a deposition temperature of 230 °C under a deposition pressure of 3 Torr. The impurity contents of Ir and IrO_2 were under an AES detection limit.

ACKNOWLEDGMENTS

This work was supported by the Korea Research Foundation Grant funded by the Korean Government (MOEHRD, Basic Research Promotion Fund) (KRF-2005-005-J09702).

[1] G. W. Dietz, W. Antpohler, M. Klee, and R. Waser, J. Appl. Phys. **78**, 6113 (1995).
[2] G. W. Dietz, M. Schumacher, R. Waster, S. K. Streiffer, C. Basceri, and A. Kingon, J. Appl. Phys. **82**, 2359 (1997).
[3] C. H. Lin, P. A. Friddle, X. Lu, H. Chen, Y. Kim, and T. B. Wu, J. Appl. Phys. **88**, 2157 (2000).
[4] B. K. Moon, K. Hironaka, C. Isobe, and S. Hishikawa, J. Appl. Phys. **89**, 6370 (2001).
[5] A. Grill, W. Kane, J. Viggiano, M. Brady, and R. Laibowitz, J. Mater. Res. **7**, 3260 (1992).
[6] S. Ezhilvalavan and T. Y. Tesng, Mater. Chem. Phys. **65**, 227 (2000).
[7] Y. Matsui, M. Hiratani, and S. Kimura, Jpn. J. Appl. Phys., Part 1 **39**, 256 (2000).
[8] C. B. Alock and G. W. Hooper, Proc. R. Soc. London, Ser. A **254**, 551 (1960).
[9] M. Ritala, M. Leskelä, J. P. Dekker, C. Mutsaeres, P. J. Soininen, and J. Skeap, Chem. Vap. Deposition **5**, 7 (1999).
[10] J. W. Lim, H. S. Park, and S. W. Kang, J. Electrochem. Soc. **148**, C403 (2001).
[11] T. Aaltonen, M. Ritala, V. Sammelselg, and M. Leskelä, J. Electrochem. Soc. **151**, G489 (2004).
[12] T. Aaltonen, M. Ritala, Y. L. Tung, Y. Chi, K. Arstila, K. Meinander, and M. Leskelä, J. Mater. Res. **19**, 3353 (2004).
[13] Y. Park, J. H. Lee, J. M. Koo, S. P. Kim, S. Shin, C. R. Cho, and J. K. Lee, Integr. Ferroelectr. **66**, 85 (2004).
[14] S. Choi, Y. K. Cha, B. S. Seo, S. Park, J. H. Park, S. Shin, K. S. Seol, J. B. Park, Y. S. Jung, Y. Park, Y. Park, I. K. Yoo, and S. H. Choi, J. Phys. D **40**, 1426 (2007).
[15] J. H. Kim, D. S. Kil, S. J. Yeom, J. S. Roh, N. J. Kwak, and J. W. Kim, Appl. Phys. Lett. **91**, 052908 (2007).
[16] M. Shimizu, K. Kita, H. Fujisawa, N. Tomozawa, and H. Niu, Proceedings of the 12th IEEE International Symposium on the Application of Ferroelectrics, 2000, p. 961 (unpublished).
[17] H. Fujisawa, S. Watari, N. Iwamoto, M. Shimizu, H. Niu, and N. Oshima, Integr. Ferroelectr. **68**, 85 (2004).
[18] R. S. Chen, Y. S. Chen, Y. S. Huang, Y. L. Chen, Y. Chi, C. S. Liu, K. K. Tiong, and A. J. Carty, Chem. Vap. Deposition **9**, 301 (2003).
[19] S. Y. Cha and H. C. Lee, Jpn. J. Appl. Phys., Part 2 **38**, L1128 (1999).
[20] K. M. Byun and W. J. Lee, Jpn. J. Appl. Phys., Part 1 **43**, 2655 (2004).